



HAL
open science

Aqueous photodegradation of the benzophenone fungicide metrafenone: Carbon-bromine bond cleavage mechanism

Minghui Hong, Xuerui Yang, Xuwei Zhang, Yuefei Ji, Lei Zhou, Guangli Xiu, Zhigang Ni, Claire Richard

► **To cite this version:**

Minghui Hong, Xuerui Yang, Xuwei Zhang, Yuefei Ji, Lei Zhou, et al.. Aqueous photodegradation of the benzophenone fungicide metrafenone: Carbon-bromine bond cleavage mechanism. *Water Research*, 2021, 206, pp.117775. 10.1016/j.watres.2021.117775 . hal-03407878

HAL Id: hal-03407878

<https://hal.science/hal-03407878v1>

Submitted on 28 Oct 2021

HAL is a multi-disciplinary open access archive for the deposit and dissemination of scientific research documents, whether they are published or not. The documents may come from teaching and research institutions in France or abroad, or from public or private research centers.

L'archive ouverte pluridisciplinaire **HAL**, est destinée au dépôt et à la diffusion de documents scientifiques de niveau recherche, publiés ou non, émanant des établissements d'enseignement et de recherche français ou étrangers, des laboratoires publics ou privés.

1 Aqueous photodegradation of the benzophenone fungicide
2 metrafenone: Carbon-bromine bond cleavage mechanism

3 Minghui Hong ^a, Xuerui Yang ^a, Xuewei Zhang ^a, Yuefei Ji ^b, Lei Zhou ^{a*}, Guangli

4 Xiu ^a, Zhigang Ni ^c, Claire Richard ^d

5

6 ^a State Environmental Protection Key Lab of Environmental Risk Assessment and
7 Control on Chemical Processes, School of Resources & Environmental Engineering,
8 East China University of Science and Technology, Shanghai 200237, China

9 ^b College of Resources and Environmental Sciences, Nanjing Agricultural
10 University, Nanjing, 210095, China

11 ^c College of Material, Chemistry and Chemical Engineering, Hangzhou Normal
12 University, Hangzhou 311121, China

13 ^d Université Clermont Auvergne, CNRS, Sigma-Clermont, Institut de Chimie de
14 Clermont-Ferrand, F-63178 Aubière, France

15

16 *Corresponding author.

17 Email address: zhoulei@ecust.edu.cn

18

19

20

21

22 **Abstract**

23 Metrafenone (MF), as a new type of benzophenone fungicide, has been widely
24 used in agriculture and is persistent in the environment. Understanding its
25 photochemical fate is essential for the comprehensive evaluation of its ecological risk.
26 In the present work, we reported a detailed study on the photochemical transformation
27 of MF in aqueous solution under irradiation (at $\lambda > 290$ nm using a high pressure
28 mercury lamp). MF was relatively photo-reactive showing a low polychromatic
29 quantum yield of photolysis (1.06×10^{-4}) counterbalanced by a significant light
30 absorption above 290 nm. A series of photoproducts were identified by high
31 resolution mass spectrometry (HR-MS) analysis, and three different pathways,
32 including oxidation of the methyl group, debromination and replacement of bromine
33 by hydroxyl group were proposed. Among them, debromination was identified as the
34 dominating process that could be achieved *via* homolytic C-Br bond cleavage from
35 singlet and triplet MF, as confirmed by laser flash photolysis (LFP) experiments and
36 density functional theory (DFT) calculations. Toxicity assessment revealed that
37 photochemical degradation reduced the ecotoxicity of MF efficiently. Nitrate ions and
38 humic acid promoted the MF photolysis, while bicarbonate exhibited no effect.
39 Results obtained in this work would increase our understanding on the environmental
40 fate of MF in sunlit surface waters.

41 **Keywords:** Metrafenone; Photolysis; Debromination; Homolytic cleavage; Bond
42 dissociation energy.

43 **1. Introduction**

44 Fungicides are widely applied to control fungal pathogens on growing crops to
45 improve yields (Cintia et al., 2021; Lin et al., 2020; Miller et al., 2021; Nermine et al.,
46 2021; Patrick et al., 2021; Regueiro et al., 2015). Metrafenone (MF) is a new type of

47 benzophenone derivative fungicide, which is a brand-new active ingredient in the
48 field of phytochemical protection (structure in Fig. 1). Studies have demonstrated that
49 MF is effective in reducing spore germination, preventing appressorium formation,
50 and inhibiting powdery mildew infestation (Franck et al., 2000; Krystina et al., 2006).
51 Hence, it has been widely used to prevent and treat powdery mildew in crops such as
52 wheat and grapes. However, repeated application of fungicides over a longtime period
53 would inevitably lead to their accumulation in the environment. These toxic
54 compounds can leach out of the soil, and contaminate surface water and groundwater,
55 inducing potential health risks to residents (Freya and Jane, 2004; Pimmata et al.,
56 2013). In agricultural production, MF is normally pre-applied and there is a tendency
57 to increase the amount applied as microbial resistance increases, resulting in its
58 persistence in the environment (Kunova et al., 2016; Leroux et al., 2013). Residual
59 MF has been widely detected in grapes, juices, and wines after its application to vines,
60 which eventually affect the human health (Briz-Cid et al., 2014; Cabras and Angioni,
61 2000; Noelia et al., 2018; Noguerol et al., 2010). Regueiro et al. (2015) once
62 evaluated the toxicity of MF on cortical neurons in mice, they reported that MF
63 induces depolarization of mitochondrial membranes, reduces cellular activity, and
64 exhibits toxic effects after 7 days of exposure (Regueiro et al., 2015).

65 **Fig. 1.**

66 In order to accurately assess the ecological risks of fungicides, it is essential to
67 investigate their transformation and fate in the environment (Baćmaga et al., 2019).
68 Photochemical transformation is among the most important processes that affect the

69 fate of organic compounds in surface water (Ge et al., 2009; Yong et al., 2009). Direct
70 photolysis of fungicides is caused by direct absorption of photons, while indirect
71 photolysis is triggered by the absorption of light by photosensitizers. Active
72 components in water (such as dissolved organic matter and ions) can interact with
73 organic pollutants through energy transfer of excited substances or through
74 photoproduction of reactive transient species, which affects the persistence and fate of
75 fungicides in the environment (Avetta et al., 2014; Fréneau et al., 2019; Jennifer et al.,
76 2019; Liu et al., 2016). As shown in Fig. 1, the molecular structure of MF contains
77 chromophores such as benzene rings and carbonyl groups which can absorb
78 ultraviolet or visible light, indicating that direct photolysis of MF is likely upon
79 irradiation (Turro, 1978). López-Fernández et al. (2018) confirmed that photolysis is
80 an effective route for the removal of MF from grape juice (López-Fernández et al.,
81 2018). However, to our knowledge, specific studies on the photolytic fate of MF in
82 natural surface waters is quite limited.

83 In the current study, the photolytic behavior of MF in aqueous solution is
84 investigated systematically, the main degradation pathways and mechanisms are
85 proposed. For this, steady-state irradiations are performed to measure the quantum
86 yield of MF photolysis, the second order rate constant ($k_{^1O_2, MF}$) for the reaction
87 between singlet oxygen (1O_2) and MF and test the effect of pH and quenchers. In
88 addition, laser flash photolysis (LFP) experiments are conducted to identify the
89 transient species involved in the reaction and density functional theory (DFT)
90 calculations are adopted to confirm the hypotheses. The and MF and are also

91 measured. The photodegradation products of MF are determined by high resolution
92 mass spectrometry (HR-MS) and their toxicity is evaluated by Ecological Structure
93 Activity Relationship (ECOSAR 2.0) software. Subsequently, the effects of water
94 matrices including nitrate ions, bicarbonate, and humic acid on MF photodegradation
95 are evaluated. Results obtained here will provide a scientific basis for a
96 comprehensive understanding of the photochemical fate of MF in the aquatic
97 environment.

98 **2. Materials and methods**

99 *2.1. Materials*

100 Metrafenone (MF, 99.7%) and humic acid (HA, 99%) were purchased from
101 Sigma-Aldrich (St. Louis, MO, USA). Phosphoric acid with chromatographic purity
102 and sorbic acid (99.8%) were obtained from Aladdin (Shanghai, China). Deuterium
103 oxide (D₂O, 99.9%) was obtained from Energy Chemical (Shanghai, China).
104 Isopropanol (IPA, 99.9%) was obtained from Thermo Fisher Scientific (Waltham,
105 USA). Sodium nitrate (≥98.5%) and sodium bicarbonate (≥99.5%) were purchased
106 from Sinopharm Chemical Reagent Co., Ltd and Richjoint, respectively. HPLC grade
107 acetonitrile (ACN, 99%) was obtained from J&K Scientific Ltd (Shanghai, China).
108 Other reagents were at least of analytical grade and used as received.

109 *2.2. Photolysis experiments*

110 *2.2.1 Steady-state photolysis experiments*

111 Steady-state photolysis experiments were conducted in a device equipped with a
112 500 W high pressure mercury lamp (Beijing Zhongjiao Jinyuan Technology Co., Ltd,

113 China) surrounded by a 290 nm cut-off filter as the light source. The mercury lamp
114 was turned on preliminarily for 30 min. After stabilization, 25 mL solution to be
115 irradiated containing target compounds (20 μ M) were pipetted into a Pyrex glass
116 reactor. During the irradiation process, Pyrex glass reactors were transferred to the
117 water-cooled immersion well in the device to maintain the temperature at 20 $^{\circ}$ C. Dark
118 controls were also performed under the same conditions. During the irradiated process,
119 0.5 mL aliquot of the solution to be irradiated was withdrawn at predetermined time
120 intervals for analysis. To ensure the reliability of the data, all experiments were
121 carried out at least in duplicates, and the error bars in the figures represent the
122 standard deviation (SD).

123 *2.2.2 Laser flash photolysis experiments*

124 Laser flash photolysis (LFP) experiments were carried out using a Quanta Ray
125 LAB-150–10 Nd:YAG laser at an excitation wavelength of 266 nm to investigate the
126 absorbance and disappearance of the transient species in ACN solutions of MF.
127 Solutions were purged with purified N₂ prior to the experiments to evaluate the effect
128 of O₂ (triplet quencher) on the lifetime of transient species. Different time windows
129 were used to fit the decay of the transient species of MF.

130 *2.3. Analytical methods*

131 The concentration of MF was measured using a high performance liquid
132 chromatograph (HPLC, Waters) equipped with a separation module (Waters 2695)
133 and a photodiode array detector (Waters 2998). Detailed operation conditions are
134 provided in Text. S1.

135 The transformation products were identified by a high resolution mass
136 spectrometry (HR-MS), which was coupled to a HPLC Waters Alliance system for
137 chemical separation. The details of HR-MS analysis are given in Text. S2.

138 The bromine ion concentration was measured by ion chromatograph and the
139 details are provided in Text. S3.

140 The details for electron paramagnetic resonance spectroscopy analysis (EPR) are
141 illustrated in Text. S4.

142 *2.4 Quantum yield*

143 The polychromatic quantum yields of MF (Φ_{MF}) direct photolysis in aqueous
144 solutions were determined using *p*-nitroanisole (PNA)/pyridine (pyr) as an
145 actinometer according to Eq. (1).

$$146 \quad \Phi_{\text{MF}} = \frac{k_{\text{MF}}}{k_{\text{PNA}}} \times \frac{\sum_{\lambda} (L_{\lambda} \varepsilon_{\lambda, \text{MF}})}{\sum_{\lambda} (L_{\lambda} \varepsilon_{\lambda, \text{PNA}})} \times \Phi_{\text{PNA}} \quad (1)$$

147 where k_{MF} and k_{PNA} were the observed photolysis rate constant of MF and PNA,
148 respectively. ε_{λ} ($\text{mol}^{-1} \text{cm}^{-1}$) represented the molar absorptivity and L_{λ} ($\text{cm}^{-2} \text{s}^{-1}$) was
149 the incident light intensity. $\sum_{\lambda} (L_{\lambda} \varepsilon_{\lambda, \text{MF}})$ and $\sum_{\lambda} (L_{\lambda} \varepsilon_{\lambda, \text{PNA}})$ were the light absorption
150 for MF and actinometer, respectively. Φ_{PNA} was the quantum yield of PNA and was
151 calculated according to $\Phi_{\text{PNA}} = 0.29[\text{pyr}] + 0.00029$ (Laszakovits et al., 2016). The ε_{λ}
152 values of aqueous MF and PNA solutions were measured using a UV-Vis
153 spectrophotometer and specific pathlength quartz cells.

154 *2.5. DFT calculations*

155 In this study all the density functional theory (DFT) calculations were conducted
156 by using Gaussian 16 package with hybrid density functional B3LYP method. The

157 details for DFT calculation were illustrated in Text. S6.

158 2.6. Ecotoxicity assessment

159 The aquatic toxicity data was an essential judgment basis for environmental
160 hazard classification and ecological risk assessment of chemicals (Cash, 1998). In the
161 present study, the ecotoxicity of MF and photoproducts was evaluated by the
162 Ecological Structure Activity Relationship (ECOSAR 2.0). Three classical aquatic
163 organisms (green algae, daphnia and fish) were assessed for acute toxicity (half-lethal
164 and half-effect concentration (LC50, EC50)) and chronic toxicity values (Chv) (Wang
165 et al., 2019).

166 3. Results and discussion

167 3.1 Direct photolysis of MF

168 The UV-Vis absorption spectrum of aqueous MF exhibits a broad absorption
169 band ranging from 260 to 350 nm ($\lambda_{\max} = 292$ nm, $\epsilon_{292} = 7750$ mol⁻¹ cm⁻¹) thus well
170 overlapping with the emission spectrum of the mercury lamp (Fig. 2) and of the solar
171 spectrum, implying that direct photodegradation can potentially take place for MF in
172 natural conditions. The absorption band of MF is mainly due to the presence of
173 chromophores such as benzene and ketone groups that are capable of absorbing
174 UV-Vis light. In the present study, the absorption band corresponds to the low energy
175 $\pi \rightarrow \pi^*$ excitation due to the presence of the benzene chromophore rather than the
176 ketone chromophore ($n \rightarrow \pi^*$ excitation) (Turro, 1978). This could be further
177 confirmed by TD-DFT calculations, as shown in Fig. S1, the broad band ranging from
178 260 nm to 350 nm is attributed to the S1 to S5 absorptions, among which the S4 state

179 has the largest oscillator strength (Table. S1). We thus analyzed the molecular orbital
180 (MO) transition contributions of the S4 state. The two main transitions are the highest
181 occupied molecular orbital (HOMO)-2 to the lowest unoccupied molecular orbital
182 (LUMO) and HOMO-1 to LUMO. Based on the isosurfaces of HOMO-2 (π),
183 HOMO-1 (π), and LUMO (π^*) (Fig. S2), the excitation can be assigned to a $\pi \rightarrow \pi^*$
184 transition. In addition, solvatochromic experiments by using ACN as a solvent could
185 also demonstrate this phenomenon of absorption band distribution (Fig. 2). Molecules
186 that undergo a $\pi \rightarrow \pi^*$ transition are believed to have excited states more strongly
187 polarized than the ground state. Therefore, a strongly polar solvent (such as water) has
188 a greater stabilizing effect on the excited state and can reduce the energy difference
189 between the excited state and the ground state. Therefore, as polarity of the solvent
190 decreased with the solvent substitution of H₂O by ACN, the absorption was
191 hypochromatically shifted, which implied that the energy required from the ground
192 state to the excited state became larger, demonstrating that the MF molecule
193 underwent a $\pi \rightarrow \pi^*$ transition (Da et al., 2001). The $n \rightarrow \pi^*$ excitation was not
194 observed (or was weak) because of the poor spatial overlap of the n and π^* orbitals,
195 resulting in a weak vibronic intensity, which should theoretically be at 350 nm (Lim
196 and Jack, 1966).

197 **Fig. 2.**

198 Dark control experiments showed no loss of MF, therefore, hydrolytic or
199 microbial degradations were not further considered in this study. Upon irradiation, a
200 significant MF decay was observed, implying that photolysis limited the persistence

201 of MF in aqueous solutions. The decay of MF could be fitted by a pseudo-first-order
202 kinetics, and the observed rate constant (k_{obs}) was calculated by linear regression of
203 logarithmic concentration values ($\ln([\text{MF}]_t / [\text{MF}]_0)$) determined as a function of time
204 (Eq. (2)). Half-life ($t_{1/2}$) was also calculated according to Eq. (3). In the present work,
205 k_{obs} was determined to be $0.056 \pm 0.003 \text{ h}^{-1}$ under simulated sunlight, corresponding
206 to a half-life ($t_{1/2}$) of $12.4 \pm 0.6 \text{ h}$. These values were comparable with that reported
207 values ($0.072 \pm 0.005 \text{ h}^{-1}$ (k_{obs}) and $9.6 \pm 0.7 \text{ h}$ ($t_{1/2}$)) (López-Fernández et al., 2018).
208 European Food Safety Authority (EFSA) concluded that the half-life of MF in the
209 dark aerobic water sediment system (biological degradation) is 8.5-9.2 days (EFSA.,
210 2006). It clearly shows that MF is difficult to biodegrade, therefore, we can conclude
211 that photolysis plays an important role in the elimination of MF in the aquatic
212 environment.

$$213 \quad \ln([\text{MF}]_t / [\text{MF}]_0) = -k_{\text{obs}}t \quad (2)$$

$$214 \quad t_{1/2} = \ln 2 / k_{\text{obs}} \quad (3)$$

215 Quantum yields are important parameters in photochemistry. The quantum of a
216 given process or of a global reaction corresponds to the ratio of photons triggering a
217 photochemical process or the reaction to the total number of absorbed photons (Rene,
218 2002) and therefore gives the efficiency of absorbed photons to achieved the process
219 or the reaction. Here, the polychromatic quantum yield of MF photolysis (Φ_{MF}) at 20
220 μM was determined to be 1.06×10^{-4} , which is higher than the quantum yields of
221 photolysis of other benzophenone derivatives that do not contain halogene atoms such
222 as benzophenone-3 (1.51×10^{-5}) and 4-hydroxy-benzophenone (7.91×10^{-6}) (Li et al.,

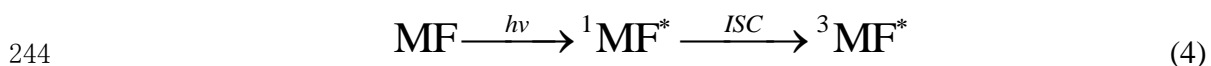
223 2016). This result suggests that the presence of a Br atom in MF may favor the
224 photodegradation.

225 The potential impact of pH solution on MF photolysis was also tested. Our results
226 indicated that the rate of photodegradation was barely affected by the solution pH
227 between 4 and 10 (Fig. S4). This phenomenon is reasonable based on the
228 pH-independent absorption spectra of MF (Fig. S5) and on the absence of dissociable
229 functional groups in the molecular structure of MF.

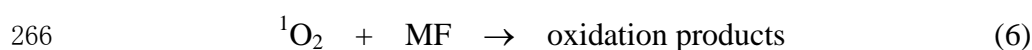
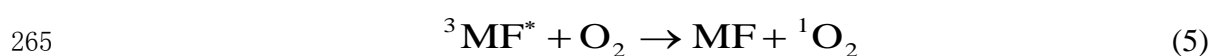
230 *3.2 Identification of potential reactive intermediates*

231 The triplet excited state of carbonyls has attracted a wide interest as a special
232 oxidant in photochemical reactions. Upon irradiation, MF molecules were likely to
233 absorb photons to make an energy level transition from the ground state to the singlet
234 excited state ($^1\text{MF}^*$), followed by an intersystem crossing (ISC) process to generate
235 the triplet excited state ($^3\text{MF}^*$ containing two electrons with the same spin direction
236 and unpaired) (Eq. (4)) (Nicholas et al., 2012).

237 The presence of a bromine atom in MF molecule is expected to enhance the
238 spin-orbit coupling due to the heavy halogen effect, thus favoring the ISC process.
239 Therefore, the generation of $^3\text{MF}^*$ and its involvement in the photolysis process is
240 likely. Sorbic acid (a triplet excited state quencher) was added to the MF solution to
241 test the involvement of $^3\text{MF}^*$ (Zhou et al., 2013). As shown in Fig. 3, the presence of
242 sorbic acid (0.4 mM) partially inhibited the reaction, confirming the involvement of
243 $^3\text{MF}^*$ in the photo-transformation.



245 It has been reported that the energy required to excite many aromatic compounds to
246 their triplet excited states was greater than 250 kJ mol⁻¹, whereas the energy for ¹O₂
247 formation was only 94 kJ mol⁻¹ (Zepp et al., 1987). Therefore, under irradiation,
248 energy transfer between the triplet excited state of organic compounds and dissolved
249 oxygen may occur, resulting in the production of ¹O₂. For example, the triplet excited
250 state energy of benzophenone was as high as 288 kJ mol⁻¹, which was sufficient to
251 transfer energy to dissolved oxygen and generate ¹O₂ with a quantum yield of 0.34
252 (Turro et al., 2012). Since replacing H₂O with D₂O extends the lifetime of ¹O₂ 13-fold
253 (Rodgers and Snowden, 1982) a D₂O-H₂O mixture (50:50, v:v) was employed as a
254 solvent to investigate whether ¹O₂ was produced in the reaction and was responsible
255 for MF oxidation. The reaction rate constant increased by a factor of 1.64 when the
256 solvent was changed to the mixture of D₂O-H₂O (Fig. 3), indicating that ¹O₂ was
257 generated in the photolysis of MF by photosensitization. Therefore, these results are
258 consistent with the formation of ³MF* and the generation of ¹O₂ by energy transfer to
259 O₂ (Eq. (4) and (5)). Once formed, ¹O₂ could react with MF (Eq (6)). We therefore
260 further measured the bimolecular rate constant of this reaction, $k_{^1O_2, MF}$. The value
261 found: 5.6 × 10⁷ L mol⁻¹ s⁻¹ demonstrated the easy oxidation of MF by ¹O₂.
262 Furthermore, the irradiation of MF in the presence of isopropanol (0, 8 and 20 mM)
263 used as an •OH radical scavenger ruled out the involvement of this radical in the
264 photolysis of MF (Fig. S6).



267

268

Fig. 3.

269

270 In the case MF disappears through Eq (6), the rate of MF loss can be written:

271
$$-d[\text{MF}]/dt = I_a \times \Phi_{\text{SO}} \times (k_{1\text{O}_2,\text{MF}} \cdot [\text{MF}] / (k_{1\text{O}_2,\text{MF}} \cdot [\text{MF}] + k_d) \quad (7)$$

272 Where I_a is the rate of light absorption by MF, Φ_{SO} , the quantum yield of $^1\text{O}_2$
273 formation and k_d , the rate of $^1\text{O}_2$ desactivation in water ($2.5 \times 10^5 \text{ s}^{-1}$, Rodgers and
274 Snowden, 1982). Moreover, Φ_{MF} is equal to :

275
$$\Phi_{\text{MF}} = -d[\text{MF}]/dt/I_a = \Phi_{\text{SO}} \times (k_{1\text{O}_2,\text{MF}} \cdot [\text{MF}] / (k_{1\text{O}_2,\text{MF}} \cdot [\text{MF}] + k_d) \quad -(8)$$

276 It means that Φ_{MF} depends on the $[\text{MF}]$, in particular when $k_{1\text{O}_2,\text{MF}} \cdot [\text{MF}] \ll k_d$, that is
277 the case at the chosen concentrations. To check this, we measured Φ_{MF} for several
278 concentrations ranging from 20 to 5 μM . Φ_{MF} decreased from 1.06×10^{-4} for 20 μM to
279 0.52×10^{-4} for 5 μM , in accordance with a contribution of $^1\text{O}_2$ to the
280 phototransformation of MF.

281

282 M. A. J. Rodgers, P. T. Snowden. Lifetime of ($^1\text{O}_2$) in Liquid Water As Determined by
283 Time-Resolved Infrared Luminescence Measurements. J. Am. Chem. Soc. 1982,
284 104, 5541-5543. [doi-org.ezproxy.uca.fr/10.1021/ja00384a070](https://doi.org/10.1021/ja00384a070)

285

286 *3.3 Photoproducts identification*

287 In this work, we systematically investigated intermediate photoproducts of MF
288 via HR-MS analysis after 22 h irradiation. The major intermediate photoproducts are

289 listed in Table. S2. Bromine atom has two isotopes (relative atomic mass 78.9183 and
290 80.9163), based on this property, isotopic features were used as a diagnostic tool for
291 the identification of photoproducts containing bromine atoms. For instance, the parent
292 compound MF had a molecular ion cluster corresponding to $m/z = 409.0634/411.0612$
293 ($[M+H]^+$) with retention time of 4.91 min, suggesting that the molecular structure of
294 MF contained one bromine atom. Reviewing Table. S2, it can be seen that eight
295 photoproduct intermediates were detected. Specifically, TP1 with $m/z =$
296 $423.0426/425.0404$ ($[M+H]^+$) at retention time of 1.97/2.65 min was assigned as the
297 oxidation product in which a methyl group was oxidized into aldehyde. The $m/z =$
298 $439.0375/441.0353$ ($[M+H]^+$) molecular ion was labeled as the secondary product
299 (TP2), which was generated by oxidation of the methyl group to carboxyl with
300 retention time of 1.28/1.6 min. Based on the total ion currents (TICs), debrominated
301 product (TP3) was a major intermediate product generated during MF photolysis (Fig.
302 S7), which was eluted at 2.56 min with $m/z = 331.1530$. Furthermore,
303 debrominated-methyl oxidation products (TP4 and TP5) were identified based on m/z
304 $= 345.1325$ and 361.1273 ($[M+H]^+$) with retention time of 1.63/1.90 and 1.22/1.41
305 min, respectively. Notably, TP3, TP4 and TP5 were also observed in a previous study
306 (López-Fernández et al., 2018). Moreover, TP6 with $m/z = 347.1480$ ($[M+H]^+$) was
307 identified as the OH substitution product, which was another major debromination
308 product (Fig. S7). To the best of our knowledge, the formation of
309 debrominated-hydroxylated photoproduct in the photolysis of MF was reported for the
310 first time. TP7 and TP8 ($m/z = 361.1273$ and 377.1221 , $[M+H]^+$) were assigned to the

311 methyl oxidized from of TP6.

312 To gain deeper insight into the debromination process, the evolution of releasing
313 bromide was recorded during the photolysis of MF, and the yield of bromide was
314 calculated according to Eq. (9) (Xu et al., 2020):

$$315 \quad \text{Yield of bromide} = \frac{[\text{Br}^-]_t}{[\text{MF}]_0 - [\text{MF}]_t} \times 100\% \quad (9)$$

316 where $[\text{Br}^-]_t$ is the concentration of bromide ion detected at irradiation time t ; $[\text{MF}]_0$
317 and $[\text{MF}]_t$ are the concentrations of MF at irradiation time zero and t , respectively.

318 Based on the results of ion chromatography, we obtained an average bromine yield of
319 $73 \pm 1\%$ for MF direct photolysis (Fig. S8), which confirmed our conclusion that
320 debromination is a major pathway in the direct photolysis of MF.

321 *3.4 Photolysis pathways*

322 Based on the detected intermediates, several photodegradation pathways of MF
323 are proposed (Fig. 4). Pathway I corresponded to the oxidation of the β -methyl group,
324 giving rise to a phenylacetaldehyde product (TP1), followed by a further oxidation
325 process to convert the aldehyde group to a carboxyl group. Pathway II corresponded
326 to the debromination process, leading to the generation of TP3. It was noteworthy that
327 TP3 exhibited a relatively strong signal in the mass spectrum (Fig. S7), indicating that
328 the yield of this product was relatively high during MF photolysis. Subsequently, TP3
329 could further undergo methyl oxidation and aldehyde oxidation to produce TP4 and
330 TP5 sequentially. Such process has been previously reported by López-Fernández et
331 al. (2018) in the photolysis process of MF. Pathway III corresponded to the
332 substitution of bromine by a hydroxyl group to give TP6, then, the methyl group on

333 TP6 could sequentially be oxidized to form TP7 and TP8.

334 Furthermore, it has been well documented that for the photochemical
335 transformation of carbonyl chemicals, Norrish type I and II reactions were proposed
336 to take place through which fission of the carbon-carbon bond would occur at the α -
337 and γ -positions, leading to the formation of bond cleavage or intramolecular
338 cyclization products, respectively (Turro, 1978). However, in the present study, none
339 of the above-mentioned products were identified by mass searching from the total ion
340 chromatography (TIC) spectra; instead, the dominated photolysis pathway of MF was
341 proposed as debromination process, which would be discussed in detail in the
342 following section.

343 **Fig. 4.**

344 *3.5 Photo-induced debromination*

345 As mentioned, debrominated product (TP3) were found to be the major
346 photoproduct of MF, indicating that C-Br bond dissociation was an important path of
347 mechanistic explanation. This bond cleavage might take place either *via* a homolytic
348 process to give a carbon-based benzoylbenzyl radical and bromine atom, or through a
349 heterolytic process to generate a corresponding benzyl cation and bromide anion.

350 In order to gain a detailed insight into the photolysis mechanism of MF, LFP
351 experiments were conducted to identify the potential transient intermediates involved
352 in the photochemical process. Fig. 5 exhibited the time-dependent transient absorption
353 spectrum of 0.25 mM MF in ACN after 266 nm laser excitation. As can be seen, a
354 broad transient absorption band with maximum absorption around 345 nm was

355 obtained at the pulse end, and the presence of two different triplet scavengers, namely,
356 oxygen and acrylamide were found to hardly affect its formation, indicating that this
357 species could not be assigned to the triplet excited state of MF (Fig. S10). In
358 accordance, the triplet excited states of benzophenone (BP) and some of its
359 derivatives were reported to show maximum absorption around 525 nm (Ryuzi et al.,
360 1997) (Fig. 5(d)). We looked after a signal in this wavelength range, but absorbances
361 were very weak (Fig. 5(c)). On the other hand, the spectrum analogy of our transient
362 ($\lambda_{\max} = 345$ nm) with those of *m*-benzoylbenzyl radical (*m*-BBR, $\lambda_{\max} = 335$ nm) and
363 *p*-benzoylbenzyl radical (*p*-BBR, $\lambda_{\max} = 320$ nm) (Yamaji et al., 2007) prompted us to
364 assign it to the benzoylbenzyl radical of MF (MBR). Yamaji et al. (2007) reported that
365 upon 266 nm excitation in LFP experiments, *m*-bromomethylbenzophenone
366 (*m*-BMBP) would be excited to generate *m*-BBR, and this process could be achieved
367 via an extremely fast ω -cleavage of both lowest singlet (S1) and triplet (T1) *m*-BMBP.
368 In their case also, triplet *m*-BMBP could be hardly be detected by LFP (Yamaji et al.,
369 2007). However, differently from *m*-BBR, MBR was found to be short-lived,
370 undergoing a fast decay within 0.05 μ s to give a relatively long-lived secondary
371 intermediate (Fig. 5(a)). The shorter life-time of MBR might be attributed to the
372 presence of methyl and methoxy substituents allowing fast intramolecular reactions to
373 take place.

374 To further support the formation of MBR, DFT calculation were conducted to
375 obtain the theoretical UV-Vis absorption of two potential intermediates, namely, MBR
376 and the benzyl cation. The validation of this method was firstly checked by

377 calculating the absorption of parent MF. As seen, theoretical calculation exhibited a
378 maximum absorption peak at 290 nm (Fig. S1), which was in a good agreement with
379 the experimentally measured absorption peak at 292 nm (Fig. 2). In the case of MBR,
380 calculation showed a maximum absorption peak around 350 nm (Fig. S11), matching
381 well with the spectrum observed by LFP experiments (Fig. 5(a)). For the benzyl
382 cation, the maximum absorption was calculated to be around 460 nm. Therefore, we
383 have confirmed the homolytic cleavage of the C-Br bond of MF.

384 In addition, for the homolytic cleavage process, we further calculated the bond
385 dissociation energy (BDE) of C-Br bond on the basis of ΔH derived from
386 thermochemical parameters from the optimized MF, MBR and bromine atom at an
387 ideal condition (298.15 K and 1 atm). A BDE value for C-Br bond cleavage of MF
388 was estimated to be 67.9 kcal mol⁻¹, which was lower than that of the lowest singlet
389 state (S1, 89.1 kcal mol⁻¹) and triplet state (T1, 71.2 kcal mol⁻¹). Based on the
390 experimental and theoretical results, an energy diagram for the deactivation and bond
391 dissociation processes of excited MF is depicted in Scheme.1. Similar to *m*-BMBP,
392 the excited singlet state of MF produced an excited triplet state through intersystem
393 crossing. Alternatively, S1 and T1 state could also undergo C-Br bond cleavage to
394 produce MBR and bromine atom (Scheme. 1(a)). Bond dissociation from S1 was
395 thermodynamically more favorable than from T1, and was proposed as the dominant
396 pathway for C-Br bond cleavage.

397 Based on the products identification, DFT calculation and LFP experiments, the
398 detailed debromination mechanism can be tentatively discussed. Once MBR was

399 generated, the formation of TP3 required access to hydrogen atoms. They cannot be
400 supplied by water, while the methyl group on the ortho-position was likely to act as a
401 good hydrogen donor. In this case MBR might undergo an extremely fast
402 intramolecular rearrangement process, leading to the rapid disappearance of MBR and
403 to the formation of the corresponding secondary transient species (Fig. 5(b)). The new
404 produced intermediate can experience an intermolecular hydrogen extraction from
405 another MF molecule, giving TP3, or undergo a series of further oxidation processes
406 to generate the methyl oxidation products.

407 In conclusion, a detailed diagram of MF photolysis process is illustrated in
408 Scheme. 1(b). Specifically, upon irradiation, MF would be excited to singlet state,
409 which could either directly break the C-Br bond or undergo ISC process to give $^3\text{MF}^*$.
410 Similarly, $^3\text{MF}^*$ undergoes C-Br bond homolytic cleavage reaction to give rise to
411 MBR and $\cdot\text{Br}$. Meanwhile, $^3\text{MF}^*$ can also transfer its energy to dissolved oxygen,
412 resulting in the formation of $^1\text{O}_2$, which in turn leads to the further oxidation of MF.

413 **Fig. 5.**

414 **Scheme.1.**

415 *3.6 Toxicity prediction during MF transformation*

416 In the present study, the acute and chronic toxicity of MF and photoproducts to
417 fish, daphnia and green algae was evaluated through the ECOSAR procedure (Wei et
418 al., 2018). The toxicity was classified according to the Globally Harmonized System
419 of Classification and Labelling of Chemicals (Liu et al., 2019).

420 The acute toxicity values of MF were determined to be 1.20 mg L⁻¹, 0.88 mg L⁻¹
421 and 1.85 mg L⁻¹ for fish, daphnia and green algae, respectively. These results showed
422 that MF was toxic for aquatic species, especially with lower trophic organisms such as
423 daphnia (< 1.0 mg L⁻¹). The chronic toxicity values (Chv) of MF were predicted to be
424 0.16 mg L⁻¹, 0.17 mg L⁻¹ and 0.85 mg L⁻¹ for fish, daphnia and green algae,
425 respectively, suggesting that MF was more likely to have a chronic toxic effect on
426 organisms. Simultaneously, the trend in chronic toxicity for the three different trophic
427 levels was consistent with acute toxicity. In summary, MF was obviously toxic to
428 aquatic species and can disrupt the ecological balance of the aquatic environment,
429 thus the detection and control of MF in the environment should be given more
430 attention.

431 Predicting the toxicities of intermediate products during MF transformation was
432 also particularly important (Karci. and Akin., 2014). Therefore, we calculated the
433 toxicity changes of the intermediate products in the three MF photolysis pathways for
434 fish, Daphnia and green algae, and the results were shown in Fig. 6. In ECOSAR
435 predictions, toxicity actually decreases if the toxicity parameter (e.g., Lethal
436 Concentration 50 (LC50)) decreases by at least one order of magnitude. From this
437 perspective, the acute toxicity of intermediate products showed a decreasing trend
438 only for Daphnia. For fish, all the debromination products (TP3 and TP6) and the
439 methyl aldolization products (TP1, TP4 and TP7) were in the same order of
440 magnitude of acute toxicity as MF. However, the acute toxicity of the methyl
441 carboxylation products (TP2, TP5 and TP8) was directly decreased by two orders of

442 magnitude. The acute toxicity variation for green algae was similar with fish, but the
443 toxicity of both TP6 and TP7 in the OH-debromination pathway was one order of
444 magnitude higher than MF, indicating that toxicity was enhanced. A little different
445 from the acute toxicity, the chronic toxicity of both debromination pathways showed a
446 continuous decreasing trend only for green algae (except TP1). For fish and daphnia,
447 the chronic toxicity of TP1, TP3, TP4, TP6 and TP7 remained in the same order of
448 magnitude as MF. Aldehyde groups are known to be toxic to organisms through
449 chemical bonding with amino bearing biomolecules such as enzymes, proteins,
450 condensates, nucleic acid derivatives etc. *via* Schiff bases (Slomkowski, 1998;
451 Sokolsky et al., 2006). This might be responsible to higher toxicity of intermediate
452 products containing aldehyde groups. Notably, further oxidation of the aldehyde
453 products to the carboxylate products decreased the toxicity rapidly. All the above
454 results indicated that the toxicity of some intermediate products of three photolysis
455 pathways may maintain or even increase, but the toxicity of the final
456 carboxyl-containing product is greatly reduced, photodegradation is still a method that
457 can safely reduce the ecotoxicity of MF in aquatic environment.

458 **Fig. 6.**

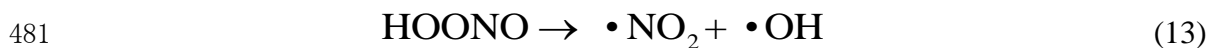
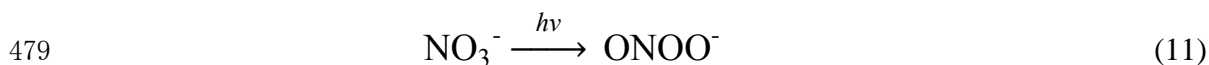
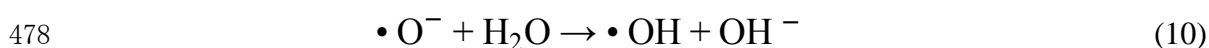
459 *3.7 Effects of natural water constituents*

460 *3.7.1 Effect of nitrate*

461 Nitrate is one of the most abundant anions in the aquatic environment whose
462 photochemical reactivity can affect the photochemical fate of the organic
463 contaminants (Mack and Bolton, 1999; Zuo et al., 2006). In the present study, the

464 photodegradation experiments of MF were conducted in 25 mL aqueous solutions
 465 containing 20 μM substrates with different nitrate concentrations (0, 5, 20 and 50 mM)
 466 under irradiation for 8 h and the results are presented in Fig. 7(a).

467 The photolysis rate of MF was observed to be significantly accelerated as the
 468 nitrate concentration increased. The rate constants were 0.055, 0.080, 0.143 and 0.167
 469 h^{-1} for nitrate concentrations of 0, 5, 20 and 50 mM, respectively. $\bullet\text{OH}$ generated by
 470 nitrate photolysis is one of the major ROS accounting for the attenuation of pollutants
 471 in natural waters (George et al., 1988; Monica et al., 2013). Eqs (9)-(13) show how
 472 solar irradiation of nitrate leads to the formation of $\bullet\text{NO}_2$ and $\bullet\text{OH}$ directly and
 473 indirectly *via* its photoisomerization to peroxyxynitrite/peroxyxynitrous acid (Kotnik et al.,
 474 2016; Vione et al., 2009). In this work, the $\bullet\text{OH}$ generated by nitrate photolysis was
 475 identified by EPR analysis (Fig. S12(a)), thus was proposed to be responsible for the
 476 decay of MF.



482 3.7.2 Effect of bicarbonate

483 Bicarbonate is the major anion responsible for water alkalinity. Bicarbonate has
 484 been reported to play an important influence on the indirect photolysis of organic
 485 pollutants in natural waters (Huang and Scott, 2000). Experimental results show that

486 the presence of bicarbonate barely affected the photolysis process of 20 μM MF (Fig.
487 7(b)). The corresponding rate constants were found to be equal to 0.059, 0.064, 0.059
488 and 0.062 h^{-1} as the bicarbonate concentration increased from 0 to 20 mM.
489 Bicarbonate can interact with $\bullet\text{OH}$ to form carbonate radicals ($\text{CO}_3\bullet^-$) (Eq. (14))
490 (Huang and Scott, 2000), which is a strong electrophile that can rapidly oxidize
491 phenolic compounds (Neta et al., 1988). However, our quenching experiments ruled
492 out the involvement of $\bullet\text{OH}$ in the direct photolysis of MF.



494 In addition, the presence of bicarbonate can also affect the photochemical
495 transformation of organic compounds *via* altering the solution pH (Ji et al., 2012).
496 However, this effect is expected to be not important due to the pH-independent
497 photolysis of MF (*vide supra*).

498 *3.7.3 Effect of humic acid*

499 Humic substances are ubiquitous in soils and surface waters which are formed by
500 decomposition of living organisms. In the aquatic environment, they are able to
501 compete with pollutants to absorb photons for photolysis as an inner filter (light
502 screener) (Luciano et al., 2009; Monica et al., 2003). Meanwhile, as a photosensitizer,
503 they are capable of affecting the persistence of organic pollutants in the environment
504 through energy transfer or reaction with photochemically produced reactive
505 intermediates (PPRI) (Manjun et al., 2006; Richard et al., 1997; Yong et al., 2009;
506 Zepp et al., 1985). In view of this, the photolysis of 20 μM MF was conducted in the
507 presence of humic acids (HA) at a concentration ranging from 0 and 20 mg L^{-1} , and

508 the results are shown in Fig. 7(c).

509 The kinetic rate constants were determined to be 0.056, 0.064, 0.094, and 0.139
510 h^{-1} at HA concentrations 0, 2, 5 and 20 mg L^{-1} , respectively. Compared with ultrapure
511 water controls, the photodegradation rate of MF in the presence of HA was
512 significantly higher. HA was a macromolecule with a complex structure, containing a
513 large number of chromophores comprised of benzene ring, carboxyl, carbonyl, and
514 methoxyl moieties (Laurentiis et al., 2013). The HA-enhanced photolysis of MF may
515 occur either through energy transfer from the excited HA to the ground state MF, or
516 *via* oxidation by PPRI, such as $\bullet\text{OH}$ and $^1\text{O}_2$, which promote the photolysis of MF
517 (Rajib et al., 2011). The involvement of $\bullet\text{OH}$ and $^1\text{O}_2$ in the photolysis of MF in the
518 presence of HA was confirmed by our EPR analyses, as illustrated in Fig. S12(b).

519 From this section, it is clear that natural water constituents such as nitrate and
520 humic acid have significant impacts on the photodegradation rate of MF. Therefore,
521 direct photolysis is not expected to be the main photodegradation pathway of MF in
522 the environment, and further studies are required to better understand its
523 photoreactivity.

524 **Fig. 7.**

525 **4. Conclusions**

526 In this study, the photodegradation of MF in aqueous solution under simulated
527 solar irradiation was investigated, including photolysis kinetics, reactive intermediates,
528 products identification, photolysis pathways and mechanisms. Under simulated sunlit,
529 direct photolysis rate constant of MF in aqueous solution was $0.056 \pm 0.003 \text{ h}^{-1}$,

530 corresponding to a half-life of 12.4 ± 0.6 h, indicating that photochemical degradation
531 was an important pathway for the removal of the fungicide MF in nature. Three
532 different pathways were proposed based on HR-MS analysis, including methyl
533 oxidation, debromination and replacement of Br by OH group. Among them
534 debromination process was identified as the main path. Homolytic cleavage of the
535 C-Br bond from both $^1\text{MF}^*$ and $^3\text{MF}^*$ is likely to take place. MF is also likely
536 oxidized by $^1\text{O}_2$ produced by energy transfer from $^3\text{MF}^*$ to O_2 . NO_3^- and humic acid
537 were found to enhance the decay of MF, while HCO_3^- exhibited no significant effect
538 on MF photolysis. Toxicity assessment revealed that photochemical transformation
539 was an efficient process to reduce the ecotoxicity of MF. This study provided
540 important information for the understanding of photolytic behavior of MF in the
541 aqueous environment.

542 **Declaration of competing interest**

543 There is no declaration of interest in this investigation. The authors declare no
544 competing financial interest.

545 **Acknowledgement**

546 This work was financially supported by the National Natural Science Foundation
547 of China (No. 22176059). The authors would also like to thank Dr. Ting Wu from
548 Research Center of Analysis and Test of East China University of Science and
549 Technology for the technical support on photoproducts identification.

550 **References**

551 Ahmad, W., Rehan Zaheer, M., Gupta, A. and Iqbal, J. 2016. Photodegradation of

552 trimeprazine triggered by self-photogenerated singlet molecular oxygen.
553 Journal of Saudi Chemical Society. 20(5), 543-546.

554 Avetta, P., Marchetti, G., Minella, M., Pazzi, M., De, L.E., Maurino, V., Minero, C.
555 and Vione, D. 2014. Phototransformation pathways of the fungicide
556 dimethomorph ((E,Z)
557 4-[3-(4-chlorophenyl)-3-(3,4-dimethoxyphenyl)-1-oxo-2-propenyl]morpholine
558), relevant to sunlit surface waters. Science of the Total Environment. 500,
559 351-360.

560 Baćmaga, M., Wyszowska, J. and Kucharski, J. 2019. The biochemical activity of
561 soil contaminated with fungicides. Journal of Environmental Science & Health,
562 Part B -- Pesticides, Food Contaminants, & Agricultural Wastes. 54(4),
563 252-262.

564 Briz-Cid, N., Figueiredo, G.M., Rial-Otero, R., Cancho, G.B. and Simal, G.J. 2014.
565 Effect of Two Anti-Fungal Treatments (Metrafenone and Boscalid Plus
566 Kresoxim-methyl) Applied to Vines on the Color and Phenol Profile of
567 Different Red Wines. Molecules. 19(6), 8093-8111.

568 Cabras, P. and Angioni, A. 2000. Pesticide residues in grapes, wine, and their
569 processing products. Journal of agricultural and food chemistry. 48(4),
570 967-973.

571 Cash, G.G. 1998. Prediction of chemical toxicity to aquatic organisms: ECOSAR vs.
572 Microtox® Assay. Environmental Toxicology. 13(3), 211-216.

573 Cintia, P., Florencia, P., Agustina, M., Belén, T., Carlos, A.P., Andrés, P.P. and Lucía, P.

574 2021. Evaluation of Fusarium mycotoxins and fungicide residues in barley
575 grain produced in Uruguay. *Journal of Agriculture and Food Research*. 3,
576 100092.

577 Da, S.J.P., Da, S.A.M., Khmelinskii, I.V., Martinho, J.M.G. and Vieira, F.L.F. 2001.
578 Photophysics and photochemistry of azole fungicides: triadimefon and
579 triadimenol. *Journal of Photochemistry and Photobiology A: Chemistry*.
580 142(1), 31-37.

581 European Food Safety Authority (EFSA). 2006. Conclusion regarding the peer
582 review of the pesticide risk assessment of the active substance metrafenone.
583 *EFSA Journal* 4(2), 1-72.

584 Franck, E.D., Joanne, G.R. and Stephen, O.D. 2000. Investigating the mode of action
585 of natural phytotoxins. *Journal of Chemical Ecology*. 26(9), 2079-2094.

586 Freya, K. and Jane, A.H. 2004. Association of pesticide exposure with neurologic
587 dysfunction and disease. *Environmental Health Perspectives*. 112(9), 950-958.

588 Frneau, M., Lefebvre, C., Gmez-Fernndez, M.A., Richard, C. and Hoffmann, N.
589 2019. Photochemical reactivity of phenyl (methyl-tetrazolyl) ketone –
590 hydrogen atom transfer vs. electron transfer. *New Journal of Chemistry*.
591 43(44), 17151-17158.

592 Ge, L.K., Chen, J.W., Qiao, X.L., Lin, J. and Cai, X.Y. 2009.
593 Light-Source-Dependent Effects of Main Water Constituent on
594 Photodegradation of Phenicol Antibiotics: Mechanism and Kinetics.
595 *Environmental Science & Technology*. 43(9), 3101-3107.

596 George, V.B., Clive, L.G., Helman, W.P. and Alberta, B.R. 1988. Critical review
597 of rate constants for reactions of hydrated electrons, hydrogen atoms and
598 hydroxyl radicals ($\cdot\text{OH}/\cdot\text{O}$) in aqueous solution. *Journal of Physical and*
599 *Chemical Reference Data*. 17(2), 513-886.

600 Huang, J.P. and Scott, A.M. 2000. Steady-state concentrations of carbonate
601 radicals in field waters. *Environmental Toxicology and Chemistry*. 19(9),
602 2181-2188.

603 Jennifer, N.A., Nicholas, C.P. and Kristopher, M. 2019. Photodegradation of
604 Fludioxonil and Other Pyrroles: The Importance of Indirect Photodegradation
605 for Understanding Environmental Fate and Photoproduct Formation.
606 *Environmental Science & Technology*. 53(19), 11240-11250.

607 Ji, Y.F., Zeng, C., Ferronato, C., Chovelon, J.M. and Yang, X. 2012.
608 Nitrate-induced photodegradation of atenolol in aqueous solution: Kinetics,
609 toxicity and degradation pathways. *Chemosphere*. 88(5), 644-649.

610 Karci. and Akin. 2014. Degradation of chlorophenols and alkylphenol ethoxylates,
611 two representative textile chemicals, in water by advanced oxidation processes:
612 The state of the art on transformation products and toxicity. *Chemosphere*. 99,
613 1-18.

614 Kotnik, K., Kosjek, T., Žegura, B., Filipič, M. and Heath, E. 2016. Photolytic fate
615 and genotoxicity of benzophenone-derived compounds and their
616 photodegradation mixtures in the aqueous environment. *Chemosphere*. 147,
617 114-123.

618 Krystina, S.O., Stefan, T., Karl-Heinz, K., Klaus, G., Harald, K. and Ralph, H. 2006.
619 Metrafenone: studies on the mode of action of a novel cereal powdery mildew
620 fungicide. *Pest management science*. 62(5), 393-401.

621 Kunova, A., Pizzatti, C., Bonaldi, M. and Cortesi, P. 2016. Metrafenone resistance
622 in a population of *Erysiphe necator* in northern Italy. *Pest Management*
623 *Science*. 72(2), 398-404.

624 Laszakovits, J.R., Berg, S.M., Anderson, B.G., O'Brien, J.E., Wammer, K.H. and
625 Sharpless, C.M. 2016. p-Nitroanisole/Pyridine and
626 p-Nitroacetophenone/Pyridine Actinometers Revisited: Quantum Yield in
627 Comparison to Ferrioxalate. *Environmental Science & Technology Letters*.
628 4(1), 11-14.

629 Laurentiis, E.D., Buoso, S., Maurino, V., Minero, C. and Vione, D. 2013. Optical
630 and Photochemical Characterization of Chromophoric Dissolved Organic
631 Matter from Lakes in Terra Nova Bay, Antarctica. Evidence of Considerable
632 Photoreactivity in an Extreme Environment. *Environmental Science &*
633 *Technology*. 47(24), 14089-14098.

634 Leroux, P., Gredt, M., Remuson, F., Micoud, A. and Walker, A.S. 2013. Fungicide
635 resistance status in French populations of the wheat eyespot fungi
636 *Oculimacula acuformis* and *Oculimacula yallundae*. *Pest Management Science*.
637 69(1), 15-26.

638 Li, Y.J., Qiao, X.L., Zhou, C.Z., Zhang, Y.N., Fu, Z.Q. and Chen, J.W. 2016.
639 Photochemical transformation of sunscreen agent benzophenone-3 and its

640 metabolite in surface freshwater and seawater. *Chemosphere*. 153, 494-499.

641 Lim, E.C. and Jack, M.H.Y. 1966. Vibronic Interaction between (n, π^*) and (π, π^*)
642 States and Spin—Orbit Coupling in Nitrogen Heterocyclics. *The Journal of*
643 *Chemical Physics*. 45(12), 4742.

644 Lin, S., Tang, T., Cang, T., Yu, S.Q., Ying, Z.T., Gu, S.J. and Zhang, Q. 2020. The
645 distributions of three fungicides in vegetables and their potential health risks
646 in Zhejiang, China: A 3-year study (2015–2017). *Environmental Pollution*. 267,
647 115481.

648 Liu, H.X., Chen, J., Wu, N.N., Xu, X.X., Qi, Y.M., Jiang, L.J., Wang, X.H. and Wang,
649 Z.Y. 2019. Oxidative degradation of chlorpyrifos using ferrate(VI):
650 Kinetics and reaction mechanism. *Ecotoxicology and environmental safety*.
651 170(15), 259-266.

652 Liu, W.R., Ying, G.G., Zhao, J.L., Liu, Y.S., Hu, L.X., Yao, L., Liang, Y.Q. and Tian, F.
653 2016. Photodegradation of the azole fungicide climbazole by ultraviolet
654 irradiation under different conditions: Kinetics, mechanism and toxicity
655 evaluation. *Journal of Hazardous Materials*. 318, 794-801.

656 López-Fernández, O., Pose-Juan, E., Yáñez, R., Rial-Otero, R. and Simal-Gándara, J.
657 2018. Modelling the isothermal degradation kinetics of metrafenone and
658 mepanipyrim in a grape juice analog. *Food Research International*. 108,
659 339-346.

660 Luciano, C., Sabrina, H., Alexandra, H., Ghislain, G., Giampietro, C., Claudio, C.,
661 Boulkamh, A. and Claire, R. 2009. Relationship between Photosensitizing

662 and Emission Properties of Peat Humic Acid Fractions Obtained by Tangential
663 Ultrafiltration. *Environmental Science & Technology*. 43(12), 4348-4354.

664 Mack, J. and Bolton, J.R. 1999. Photochemistry of nitrite and nitrate in aqueous
665 solution: a review. *Journal of Photochemistry and Photobiology. A: Chemistry*.
666 128(1), 1-13.

667 Manjun, Z., Xi, Y., Qiming, X. and Lingren, K. 2006. Photosensitized degradation
668 of bisphenol A involving reactive oxygen species in the presence of humic
669 substances. *Chemosphere*. 63(3), 378-386.

670 Miller, S.T., Sterle, D., Minas, I.S. and Stewart, J.E. 2021. Exploring fungicides
671 and sealants for management of *Cytospora plurivora* infections in western
672 Colorado peach production systems. *Crop Protection*. 146, 105654.

673 Monica, P., Fabio, T., Maria, R., Gilles, M. and Marcello, B. 2013. The impact of
674 the hydroxyl radical photochemical sources on the rivastigmine drug
675 transformation in mimic and natural waters. *Water Research* 47(14),
676 5422-5430.

677 Monica, W.L., Kathleen, T. and Scott, A.M. 2003. PhetoFate: a new approach in
678 accounting for the contribution of indirect photolysis of pesticides and
679 pharmaceuticals in surface waters. *Environmental science & technology*. 37(5),
680 899-907.

681 Nermine, V.F., Yasmeen, A.A.H., Lobna, A.H. and Miriam, F.A. 2021.
682 Determination of fungicides' residues and their degradation kinetics in orange
683 tree fruits using liquid chromatography – Tandem mass spectrometry coupled

684 with QuEChERS method. *Microchemical Journal*. 168, 106376.

685 Neta, P., Huie, R.E. and Ross, A.B. 1988. Rate constants for reactions of inorganic
686 radicals in aqueous solution. *J. Phys. Chem. Ref. Data*. 17(3), 1027–1284.

687 Nicholas, J.T., Vaidhyathan, R. and Juan, C.S. 2012. *Modern Molecular*
688 *Photochemistry of Organic Molecules. Photochemistry and Photobiology*.
689 88(4), 1033.

690 Noelia, B.C., Laura, C.S., Raquel, R.O., Beatriz, C.G. and Jesús, S.G. 2018.
691 Fungicide residues affect the sensory properties and flavonoid composition of
692 red wine. *Journal of Food Composition and Analysis*. 66, 185-192.

693 Noguerol, P.R., Gonzalez-Rodriguez, R.M., Gonzalez-Barreiro, C., Cancho-Grande, B.
694 and Simal-Gandara, J. 2010. Influence of tebuconazole residues on the
695 aroma composition of Mencia red wines. *Food Chemistry*. 124(4), 1525-1532.

696 Patrick, B., Jochen, P.Z., Marco, K., Nina, R., Thu, H.N., Verena, C.S., Christiane, B.,
697 Ralf, S. and Mirco, B. 2021. Environmentally relevant fungicide levels
698 modify fungal community composition and interactions but not functioning.
699 *Environmental Pollution*. 285(15), 117234.

700 Pimmata, P., Reungsang, A. and Plangklang, P. 2013. Comparative bioremediation
701 of carbofuran contaminated soil by natural attenuation, bioaugmentation and
702 biostimulation. *International Biodeterioration & Biodegradation*. 85, 196-204.

703 Rajib, R.C., Paul, A.C. and Madhumita, B.R. 2011. Photodegradation of
704 17 β -estradiol in aquatic solution under solar irradiation: Kinetics and
705 influencing water parameters. *Journal of Photochemistry and Photobiology A:*

706 Chemistry. 219(1), 67-75.

707 Regueiro, J., Olgun, N., Simal, G.J. and Suol, C. 2015. Toxicity evaluation of new
708 agricultural fungicides in primary cultured cortical neurons. *Environmental*
709 *Research*. 140, 37-44.

710 Rene, P.S. 2002. *Environmental Organic Chemistry*. Wiley-Interscience.

711 Richard, C., Vialaton, D., Aguer, J.P. and Andreux, F. 1997. Transformation of
712 monuron photosensitized by soil extracted humic substances: energy or
713 hydrogen transfer mechanism. *Journal of Photochemistry and Photobiology. A:*
714 *Chemistry*. 111(1), 265-271.

715 Ryuzi, K., Masahiro, K., Yoshinori, H. and Tadashi, O. 1997. Triplet exciton
716 formation in a benzophenone single crystal studied by picosecond
717 time-resolved absorption spectroscopy. *Chemical Physics Letters*. 264(6),
718 631-635.

719 Slomkowski, S. 1998. Polyacrolein containing microspheres: synthesis, properties
720 and possible medical applications. *Progress in Polymer Science*. 23(5),
721 815-874.

722 Sokolsky, P.M., Domb, A.J. and Golenser, J. 2006. Impact of aldehyde content on
723 amphotericin B-dextran imine conjugate toxicity. *Biomacromolecules*. 7(5),
724 1529-1535.

725 Turro, N.J. 1978. *Modern Molecular Photochemistry*. Benjamin Cummings
726 Publishing Co, Inc.

727 Turro, N.J., Vaidhyathan, R. and Juan, C.S. 2012. *Modern Molecular*

728 Photochemistry of Organic Molecules. Photochemistry and Photobiology.
729 88(4), 1033.

730 Vione, D., Khanra, S., Man, S.C., Maddigapu, P.R., Das, R., Arsene, C., Olariu, R.I.,
731 Maurino, V. and Minero, C. 2009. Inhibition vs. enhancement of the
732 nitrate-induced phototransformation of organic substrates by the bulOH
733 scavengers bicarbonate and carbonate. Water research. 43(18), 4718-4728.

734 Wang, M.J., Xiang, X.Y., Zuo, Y.G., Peng, J.B., Lu, K., Caroline, D., Liu, P. and Gao,
735 S.X. 2020. Singlet oxygen production abilities of oxidated aromatic
736 compounds in natural water. Chemosphere. 258, 127308.

737 Wang, Y., He, L., Lv, G.C., Liu, W., Liu, J.S., Ma, X.H. and Sun, X.M. 2019.
738 Distribution, transformation and toxicity evaluation of
739 2,6-Di-tert-butyl-hydroxytotulene in aquatic environment. Environmental
740 Pollution. 255(2), 113330.

741 Wei, B., Sun, J.F., Mei, Q. and He, M.X. 2018. Mechanism and kinetic of nitrate
742 radical-initiated atmospheric reactions of guaiacol (2-methoxyphenol).
743 Computational and Theoretical Chemistry. 1129, 1-8.

744 Xu, H.Y., Li, Y.Y., Lu, J.X., Lu, J.H., Zhou, L., Chovelon, J.M. and Ji, Y.F. 2020.
745 Aqueous photodecomposition of the emerging brominated flame retardant
746 tetrabromobisphenol S (TBBPS)*. Environmental pollution 271, 116406.

747 Yamaji, M., Ogasawara, M., Kikuchi, K., Nakajima, S., Tero-Kubota, S., Marciniak,
748 B. and Nozaki, K. 2007. Photoinduced w-bond dissociation of
749 m-halomethylbenzophenones studied by laser photolysis techniques and DFT

750 calculations. Substituted position effects. *Physical Chemistry Chemical Physics*.
751 9(25), 3268-3275.

752 Yong, C., Chun, H., Xue, X.H. and Jiu, Q. 2009. Indirect Photodegradation of
753 Amine Drugs in Aqueous Solution under Simulated Sunlight. *Environmental*
754 *science & technology*. 43(8), 2760-2765.

755 Zepp, R.G., Hoigne, J. and Bader, H. 1987. Nitrate-induced photooxidation of
756 trace organic chemicals in water. *Environ. Sci. Technol.* 21(5), 443-450.

757 Zepp, R.G., Schlotzhauer, P.F. and Sink, R.M. 1985. Photosensitized
758 transformations involving electronic energy transfer in natural waters: role of
759 humic substances. *Environ. Sci. Technol.* 19(1), 74-81.

760 Zhou, L., Ji, Y.F., Zeng, C., Zhang, Y., Wang, Z.Y. and Yang, X. 2013. Aquatic
761 photodegradation of sunscreen agent p-aminobenzoic acid in the presence of
762 dissolved organic matter. *Water Research*. 47(1), 153-162.

763 Zuo, Y., Wang, C. and Van, T. 2006. Occurrence and photochemical degradation
764 of 17 α -ethinylestradiol in Acushnet River Estuary. *Chemosphere*. 63(9),
765 1583-1590.